Materials Advances

ROYAL SOCIETY OF CHEMISTRY

PAPER

View Article Online
View Journal | View Issue

Cite this: *Mater. Adv.*, 2024, 5, 570

Thermoresponsive and biocompatible poly(*N*-isopropylacrylamide)–cellulose nanocrystals hydrogel for cell growth†

Anna Trubetskaya, *[ab] Jenni Leppiniemi, [cd] Sami Lipponen, [e] Salvatore Lombardo, [f] Wim Thielemans, [f] Thaddeus Maloney, [g] Timo Pääkkönen, [h] Kavindra Kumar Kesari, [i] Janne Ruokolainen, [i] Vesa P. Hytönen [cd] and Eero Kontturi *[j]

We describe herein a poly(*N*-isopropylacrylamide) (PNIPAAm)–cellulose nanocrystals (CNC) hydrogel as thermoresponsive and biocompatible material. The hydrogel was generated with simple and robust mixing without need for complicated derivatization. The composition of the hydrogel was optimized for good stiffening and its biocompatibility was verified with fibroblast cells. The hydrogel was prepared using an osmotic dehydration method by tuning its water content and porosity without the incorporation of additional cross-linkers. The interaction of PNIPAAm and CNC was supported by the formation of a small endotherm at 30.5–33.5 °C observed with differential scanning calorimetry and a negative value for the enthalpy during the adsorption of both compounds by the isothermal titration calorimeter. The resulting PNIPAAm–CNC hydrogel (0.25 wt%; 0.5 wt%) showed better compatibility with fibroblasts than 0.5 wt% CNC alone. Our preliminary data indicates that it is possible to use the thermoresponsive characteristics of the material to influence cell behavior by temperature changes. PNIPAAm–CNC hydrogel offer a platform for the development of versatile and affordable plant-based materials for controllable 3D cell culture and the thermoresponsive nature of the material may help to develop novel applications for example in 3D-printing.

Received 2nd August 2023,
Accepted 28th November 2023

DOI: 10.1039/d3ma00495c

rsc.li/materials-advances

Introduction

Thermal response is a widely researched quality of many systems from smart materials for drug delivery to hydrogels for biosensing.[1–4] Within soft materials, poly(*N*-isopropylacrylamide) (PNIPAAm) has achieved a cliché status among thermally responsive polymers. Exhibiting relatively lower critical solution temperature (LCST) at *ca.* 32 °C,[5] it has been popular particularly in biomedical systems because the polymer dispersion is fluid at room temperature and a gel at body temperature. PNIPAAm hydrogels with marked stiffening above the LCST have been reported in abundance.[6–10] Usually, the PNIPAAm functionalized hydrogels are based on covalent chemistry with underpinnings that may often be environmentally unsustainable.[11] In this study, we present cellulose nanocrystals (CNCs) as alternative, physical cross linkers to stiffen PNIPAAm hydrogels. CNCs are renewable nanorods, derived from plant fibers, and they possess properties that have rendered them a popular material within the past two decades: high strength coupled with low density, chirality, and susceptibility to form liquid crystals.[12]

When nanoparticles, including CNCs, are incorporated in a PNIPAAm hydrogel, they are usually chemically cross-linked to the polymer with, *e.g.*, sophisticated *graft*-polymerization routes – just as the PNIPAAm chains are cross-linked with each other in monocomponent hydrogels. Instead of a covalent approach, we have used CNCs as non-covalent cross linkers based on the tendency of polymers to adsorb at virtually any interface. Because

[a] *Department of Biosciences, Nord University, Bodø, Norway. E-mail: anna.trubetskaya@nord.no*
[b] *Department of Chemistry, University of Limerick, Castrletroy, Ireland*
[c] *Faculty of Medicine and Health Technology and BioMediTech, Tampere University, 33014 Tampere, Finland*
[d] *Fimlab Laboratories, Biokatu 4, 33520 Tampere, Finland*
[e] *Polymer Technology, School of Chemical Engineering, Aalto University, 02150 Espoo, Finland*
[f] *Sustainable Materials Lab, Department of Chemical Engineering, KU Leuven, Campus Kulak Kortrijk, Etienne Sabbelaan 53, 8500 Kortrijk, Belgium*
[g] *Department of Chemical Engineering, Aalto University, 02150 Espoo, Finland*
[h] *Nordic Bioproducts Group Oy, Tietotie 1, 02150 Espoo, Finland*
[i] *Department of Applied Physics, Aalto University, School of Science, 02150 Espoo, Finland*
[j] *Department of Bioproducts and Biosystems, Aalto University, 02150 Espoo, Finland. E-mail: eero.kontturi@aalto*

† Electronic supplementary information (ESI) available. See DOI: https://doi.org/10.1039/d3ma00495c

of the high surface area of the nano-sized CNCs, the cross-linking is abundant throughout the hydrogel matrix and it can be acquired by simply mixing the aqueous PNIPAAm solution with a CNC dispersion – something that we have explored here by multiple studies on physico-chemical interactions between PNIPAAm and CNCs. PNIPAAm–CNC hydrogels at 25 °C showed a flexible structure that easily allows mixing and embedding of cells when utilizing hydrogel as a 3D cell culture scaffold.[13] A notable stiffening of the hydrogels above the LCST was also demonstrated, together with an effect on cell mobility and growth. Control for mechanical properties of the hydrogel by temperature is regarded as highly attractive in, for example, studying the cancer mechanosignaling or developing devices with controlled detachment, such as drug-releasing wound patches.[14] This study serves as a proof of concept for a new type of truly tunable thermoresponsive hydrogels for cell and artificial tissue cultivation applications, which would serve as an alternative to animal models.

Experimental section

Materials

Cellulose nanocrystals (CNC) (L: 190 ± 50 nm; d: 7 ± 5 nm) obtained from hydrochloric acid hydrolysis of hardwood were supplied by Aalto University (Finland). Poly(*N*-isopropylacrylamide) (PNIPAAm, 40 kDa), polyethylene glycol (PEG, 35 kDa), polyethyleneimine (PEI, 600 kDa) and Triton X-100 surfactant were supplied by Sigma-Aldrich, Finland. Dulbecco's Modified Eagle Medium (DMEM), sodium chloride (NaCl, 5 M) and 4-(2-hydroxyethyl)-1-piperazineethanesulfonic acid (HEPES, 1M), penicillin–streptomycin (10 000 U mL^{-1}), Gibco TrypLE™ Select enzyme, Gibco™ GlutaMax, Gibco™ fetal bovine serum (FBS) were supplied by Thermo Fisher Scientific, UK. Mouse embryonic fibroblasts (MEFs) were donated from Dr Wolfgang Ziegler. GrowDex®-T was supplied by UPM Biomedicals, Finland.

CNC preparation

1 wt% CNC dispersion containing 1.0 mmol –COOH per gram cellulose was obtained from HCl gas hydrolyzed beech wood pulp followed by TEMPO-mediated oxidation, as reported previously.[15]

Hydrogel preparation

Hydrogels were prepared at the laboratory scale using the osmotic dehydration principle (see ESI,† Fig. S-1).[16] A setup consisted of two disposable plastic cups. PEG solution was prepared simply by mixing the proper amount of solid PEG with water to obtain the desired wt%. The solution was then mixed with magnetic stirrer until the complete dissolution of PEG. One cup's bottom was cut off, and replaced by an dialysis membrane (Spectrum™ Labs Spectra/Por™ 1, UK, cut off 6–8 kDa). 15.6 mL of 10 wt% PEG solution was used as water absorbent added to the other cup with a magnetic stir bar inside, then a cup with the attached dialysis membrane was added to the PEG solution surface. In a separated batch, CNC concentrations were increased from 0.5 to 3.5 or 6 wt% with a total volume of 15.6 mL using osmotic dehydration.[16] Then, a mixture of PNIPAAm and CNCs of the adjusted concentration with a total volume of 15.6 mL was added into the cup with the attached osmotic membrane and followed by placing the whole setup on the magnetic plate with constant stirring for 24 h at room temperature. The solid content of the hydrogels was measured by drying the samples right after the dehydration in the oven at 105 °C for 24 h. The weight was recorded before and after with a balance with five significant digits. Two independent measurements were performed.

Quartz crystal microbalance with dissipation (QCM-D)

QSX 303 sensors (Biolin Scientific, Sweden) were first washed with ultrapure water for 20 min and then dried with ultraviolet-ozone for 10 min. QCM-D sensors were left overnight in the desiccator. The cleaned sensors were anchored with the layer of PEI (4 g L^{-1}). First, PEI dispersion is adsorbed, then 0.5 wt% CNC, and later, 0.1–3.5 wt% PNIPAAm was injected at 50 μL min^{-1} to adsorb until the kinetic plateau was reached. Normalized frequency shifts and dissipation energy were determined with the following method. A driving voltage was adjusted to the fundamental frequency (f_0) of 5 MHz. Frequency and dissipation changes were measured for the third, fifth, and seventh (n = 3, 5, and 7) harmonics simultaneously and normalized to the harmonic number (n).[17] Because materials that adsorb to the sensor surface induce a decrease in the resonance frequency (f), the amount of material adsorbed can be related to the change in frequency ($\Delta f/n$). The measurements were performed in duplicate.

Rheology

The rheology of hydrogels was characterized by Rheometer MCR302 (Anton Paar, Austria) equipped with a 15 mm aluminum 1° cone and a Peltier heating plate in the temperature range from 15 to 70 °C.[18] Frequency sweeps were performed at 1% strain and 0.8 rad s^{-1} strain. The low strain limit G' values were calculated from the linear elastic region between 0.1 to 1% strain. The measuring setup was covered with a sealing oil in order to prevent evaporation during the measurement. Each sample volume was 0.1 mL. Systematic measurements at fixed CNC amounts of 0.5, 3.5, and 6 wt% using 0.25 wt% PNIPAAm concentration. After injecting the hydrogel samples onto the plate, they were allowed to equilibrate for 5 min before starting the measurement. After heating samples to 70 °C, they were allowed to thermally equilibrate for 3 min.

Differential scanning calorimetry (DSC)

The melting temperature and enthalpies were measured with a Mettler Toledo DSC 821e differential scanning calorimeter. The sample (≈8–10 mg) was cooled down from 25 °C to −50 °C at −10 °C min^{-1}, after the melting endothermic was measured by heating the sample to 150 °C at 10 °C min^{-1}.

Isothermal titration calorimeter (ITC)

Calorimetric experiments were performed using a TAM III isothermal titration calorimeter (TA Instruments, USA). The experiments were performed at neutral pH in an aqueous dispersion. All samples were thoroughly degassed under vacuum while

sonicating for 15 min before the experiments. The system was equilibrated at 25 °C while stirring at 120 rpm until the baseline shift was <50 nW h^{-1}. Titrations were performed by injecting the PNIPAAm solutions (18–20 injections of 10 μL each) from the syringe into the ITC sample cell containing CNC dispersions (0.8 mL) allowing 20–30 min between injections.

A blank experiment to determine the heat of dilution was also performed at 25 °C using identical injections of PNIPAAm into ultrapure water, and all calorimetric traces were corrected for the heat of dilution by subtracting the blank from test experiments. A thermodynamic profile of binding interaction was determined by fitting the data to an independent binding site interaction model as described previously.[19]

Nonlinear regression using the Levenberg–Marquardt algorithm was used on the parameters K_a, ΔH, and n to determine the best fit to the experimental data using NanoAnalyze data analysis software (TA instruments, USA). K_a is the affinity constant, ΔH the enthalpy change, n the stoichiometry of the interaction (number of polymers/number of CNC rods). The Gibbs free energy change ΔG was calculated from the affinity constant using eqn (1) and the entropy change ΔS using eqn (2):

$$\Delta G = -RT\ln(K_a) \quad (1)$$

$$\Delta G = \Delta H - T\Delta S \quad (2)$$

ChemSketch (version 2020.2.0, Canada) was used to draw chemical structures.

Thermoporosimetry

The measurements of hydrogels in a wet state were done on a Mettler Toledo DSC 3+ (Mettler-Toledo, USA) differential scanning calorimeter (DSC) equipped with an intracooler using 40 μL aluminium pans with the sealing lids. The freezable water was crystalized in samples at −50 °C using a ramp of 20 °C min^{-1}. The temperature was then increased to −0.2 °C and held constant until the melting transition was completed. The temperature was then decreased to −50 °C using a ramp of 2 °C min^{-1} and the resulting exothermic peak was integrated to calculate the freezing bound water. Then, the temperature was increased to 60 °C at 10 °C min^{-1} to determine the total freezable water by integrating the resulting endothermic peak.

Sample preparation for cryo-TEM

PNIPAAm–CNC hydrogels were used to study the structural changes with Cryo-Transmission Electron Microscopy (Cryo-TEM) at 20°C. Sample was stored in a temperature-controlled environment. Vitrobot was used for sample preparation and to maintain the temperature of the samples before transferring them to Cryo-sections (liquid nitrogen). A drop of each hydrogel was taken on the sample holder at 20 °C and dipped into a liquid ethane–propane mixture (−180 °C) and further transferred in liquid nitrogen. Thereafter, samples were transferred into cryo-ultramicrotome through liquid nitrogen for sectioning. Before sectioning, trapezoids were made using a diamond knife on the faces of the sample droplet where sectioning was performed. Ultrathin sections of ≈200 nm from CNC hydrogels surfaces were cut at a cryogenic temperature of −170 °C with a diamond knife on a Leica Ultra-Microtome (Leica EM FC7, Germany). Sections were collected on the carbon film-coated TEM grid.

Cryo-TEM

Cryo-TEM (Jeol JEM-3200FSC, Japan) at an accelerating voltage of 300 kV was used to study the ultrathin sections of hydrogel samples. The images of sections were taken in bright field mode and using zero loss energy filtering (omega type) with a slit width of 20 eV. Images were observed under Gatan Ultrascan 4000 CCD camera. During imaging of the sections, specimen temperature inside the TEM chamber was maintained at −187 °C. Parts of the sections based on fast and slow freezing points (fast freezing: from the surface and slow freezing: from surface to inside the sample) were chosen to take the micrographs.

Osmolality of hydrogels

Similar to previous studies with CNF-based hydrogels, CNC dispersions and PNIPAAm solutions were prepared by diluting the starting materials in water, and therefore the dispersions, solutions, and PNIPAAm–CNC hydrogel had low osmolality, ranging between 2–13 mOsmol kg^{-1}. The osmolality of hydrogels was measured using Osmomat 030 osmometer (Gonotec GmbH, Germany). Concentrated 5 M NaCl and 1 M HEPES solutions were used to obtain a final concentration of 160 mM NaCl and 20 mM HEPES for balancing the osmolality of hydrogels close to that of cell culture medium (≈350 mOsmol kg^{-1} with the neutral pH ≈ 7.2–7.4).

Cell culture

The MEF cell line[20] was used for studying biocompatibility of the material as previously described. Cells were cultured in T75 flasks and maintained in high-glucose DMEM supplemented with 10% (v/v) FBS, 1% (v/v) GlutaMax, and 1% penicillin–steptomycin in a humidified incubator at 37 °C and 5% CO_2. The cells were regularly tested negative for mycoplasma contamination. MEFs between passages 10–20 were used for biocompatibility studies of hydrogels.

Biocompatibility studies

Fibroblasts were detached from the culture flask *via* enzyme (TrypLe Select, Gibco) treatment, then counted and seeded on 96 well plate at a density of 10 000 cells per well in 100 μL of cell culture medium. Two parallel plates were prepared, and cells were let to adhere and grow for 24 h in a humidified incubator at 37 °C and 5% CO_2. Each well was examined under a microscope to ensure the growth was relatively even across the whole plate. Then, cell culture medium was removed and 100 μL of "osmolality balanced" (≈350 mOsmol kg^{-1}) sample (hydrogel or chemical compound of interest) was applied on top of the cells. Samples were incubated for 20 min at 37 °C, and then 100 μL of cell culture medium was applied to the top of the sample and cell culture was continued at 37 °C. The cell viability and the cell morphology were inspected after two-hour incubation at 37 °C, and again after 24 h.

The cell viability was determined by measuring the cytoplasmic ATP content of metabolically active cells using a CellTiter-Glo® 3D Cell Viability Assay (Promega, WI, USA) according to the manufacturer's instructions. The well plate was left to equilibrate to RT for 30 min, then centrifuged at 200 × *g* for 5 min, and 100 μL of the medium was removed from the well and replaced with 100 μL of CellTiter-Glo® –reagent to lyse the cells. The plate was shaken for 5 min, centrifuged again at 200 × *g* for 5 min and then incubated for 30 min at RT. The luminescence was recorded by an Envision multilabel plate reader (PerkinElmer, MA, USA). The mean of luminescence values measured for the cell culture medium without cells was subtracted as a reference value. All samples were analyzed as triplicates, and the analysis was repeated in three parallel experiments. The relative luminescence units (RLU) indicating cell viability after two hours for medium control was normalized by setting the luminescence values to 1, and the RLU of all other samples on two hours and 24 h were normalized against the control. Triton X-100 (0.1%) was used as a negative control. Anionic nanocellulose hydrogel (aNFC GrowDex®-T) at 0.4% concentration was used as a positive control as it is meant for cell cultivation. For medium control, the cell culture medium was diluted similarly than for hydrogels using a buffer solution consisting of 160 mM NaCl and 20 mM HEPES, pH = 7. The morphology of the cells below hydrogels were inspected and recorded by Zeiss Axio Vert.A1 inverted microscope with Zeiss, Axiocam ERc 5s camera (Carl Zeiss AG, Germany) using 10× objective. Images were taken using Zeiss Zen Black software and analyzed by ImageJ (Fiji) software.

The cell proliferation was studied at different temperatures using time-lapse imaging. Fibroblasts were detached from the culture flask *via* enzyme treatment, then counted and seeded on 96 well plate at a density of 3000 cells per well in 100 μL of cell culture medium. Cells were let to adhere and grow for 24 h in a humidified incubator at 37 °C and 5% CO_2. Then the medium was removed and as a setup 1, PNIPAAm (0.25 wt%)–CNC (0.5 wt%) hydrogel or CNC (0.5 wt%) dispersion was applied on top of cells and medium was applied as a layer on top of the samples ((Fig. 7a(2)) schematic), or as a setup 2, where CNC (0.5 wt%) dispersion or PNIPAAm (0.25 wt%)–CNC (0.5 wt%) hydrogel was mixed 1 : 1 with cell culture medium and 100 μL of the mixture was applied on top of cells (see ESI,† Fig. S-2). Setup 2 was preferred over setup 1 because at 25 °C, PNIPAAm–CNC hydrogel was liquid leading to heterogenuity when cell culture medium was added. The plate was first incubated in an environmental chamber kept at 25 °C and 5% CO_2 for 2 h and phase-images were taken every 10 min using time-lapse imaging of EVOS FL auto microscope (Thermo Fisher Scientific, Waltham, MA USA). Then, to monitor the influence of temperature-mediated changes, the temperature of the chamber was increased to 37 °C and 5% CO_2 and imaging was continued with EVOS FL auto microscope for 24 h. The images were taken with 20× objective analyzed using ImageJ (Fiji) software.

Statistical analysis

The statistical significance of differences was evaluated by one-way analysis of variance (ANOVA) with Bonferronis multiple comparison test in GraphPad Prism 5.02 software. $P < 0.05$ was considered statistically significant. In all figures, ns = not significant; * = $p < 0.05$; ** = $p < 0.01$; *** = $p < 0.001$.

Results and discussion

Interaction between PNIPAAm and CNCs

Cellulose films of nanoscale thickness (1–100 nm) are transparent, smooth (roughness *circa* 2 nm), and are therefore suitable for studying interactions between CNCs and other materials (see ESI,† Fig. S-3). QCM-D method provides the data on adsorption and the time dependence of viscous and elastic properties of adsorbed PNIPAAm layers at the solid/liquid cellulose interface.[21] In this study, we used QCM-D analysis to study the binding of PNIPAAm onto CNC surface, as shown in Fig. 1.

We observed continuous decrease in resonance frequency in the QCM data, implying mass accumulation, and thus indicating that PNIPAAm adsorbs on CNCs.[22] The driving force of any polymer adsorption is entropic but the interaction between CNCs and PNIPAAm might also be driven by hydrogen bonds. Smooth dissipation signals without noise and artifacts are due

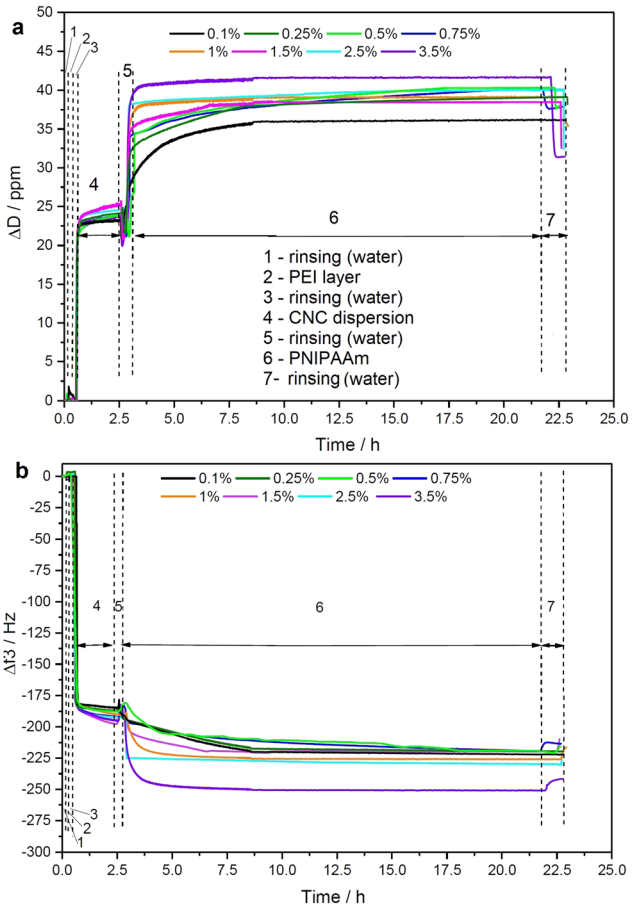

Fig. 1 Quantification of interaction between PNIPAAm and CNC using QCM-D method for hydrogels made from 0.1–3.5 wt% PNIPAAm and 0.5 wt% CNC. (a) Dissipation and (b) Frequency. The numbers mean: 1 – rinsing using DI water; 2 – PEI layer deposition; 3 – rinsing; 4 – CNCs layer deposition; 5 – rinsing; 6 – PNIPAAm layer deposition; 7 – rinsing.

to the well-controlled measurement environment during QCM runs. PNIPAAm was stirred for longer than 12 hours prior to its deposition so that a homogeneous dispersion was obtained, yielding accumulation of smooth polymer films on CNC film in the concentration range from 0.1 to 3.5 wt%. The PNIPAAm concentrations higher than of 4 wt% were not suitable for applying on QCM-D sensor due to the visible aggregation in injection tubes. ITC was used to analyze the thermodynamics of the interaction in dilute suspensions. Importantly, the ITC method provides a full thermodynamic behavior of the linkage during the adsorption including details on maximum coverage amount or the adhesion mechanism (hydrogen bonding or ionic interactions).[23]

ITC was used to shed light on the interactions leading to gelation between PNIPAAm and CNCs. Aqueous CNC dispersion was titrated with an aqueous PNIPAAm solution. An example of a calorimetric trace is shown in Fig. S-4 (ESI†), together with the calorimetric trace for the dilution of PNIPAAm to water (negative control). Both titration and dilution gave rise to exothermic peaks. The heat associated with the interaction between PNIPAAm and CNC was determined by integrating the heat associated with each titration peak and subtracting the respective heat of dilution from it. The difference between titration and dilution peaks was small but consistent and approached zero at the end of the titration, showing that the system reached saturation. Results extrapolated from fitting of the ITC data are shown in Fig. 2 and ESI† (Fig. S-5). The negative value for the enthalpy showed that binding is exothermic, which for this system, can be linked to specific hydrogen bonding between the hydroxyl and carboxylic groups of CNCs and the carbonyl oxygen or the amide group of PNIPAAm. The entropy increase can be associated with the release of surface-structured water molecules and counterions from the CNC electric double layer. This is expected as it was shown that interactions at CNC surfaces are based on enthalpy–entropy compensation of two opposite contributions, one enthalpic, related to the formation of polar interactions, and one entropic, associated with the release of water molecules from the cellulose surface.[24] For this system, both ΔH and $T\Delta S$ supply comparable contributions to the free energy of adsorption (see ESI,† Table S-1). The obtained ΔG value is in line with other studies of adsorption on cellulose surfaces.[24] Most of the published work reporting on the thermodynamics of interaction between non-ionic polymer and cellulose surfaces focused on interactions with xyloglucans. In a recent study based on molecular dynamics simulations, the authors suggest that, despite the fact that a large part of the interaction energy between charged cellulose and xyloglucan originates from hydrogen bonds, they are not the driving force of the interaction, which is linked to the increase of entropy arising from water molecules that are excluded from the respective hydration layers.[25] In the case of PNIPAAm-cellulose interactions, our findings suggest that the driving force for interaction is associated to both water exclusion (positive ΔS) and hydrogen bond formation (negative ΔH). It is possible that this difference is linked to the stronger polarization of oxygen and nitrogen in the amide group of PNIPAAm, due to resonance, resulting in a lower number of structured water molecules released from the PNIPAAm water corona upon binding, which will contribute to a more negative value of ΔH due to the lower amount of hydrogen bonds lost between PNIPAAm and bound water molecules. In addition, the water around the amide will be less structured, resulting in a lower entropy increase when releasing less water molecules. Also, xyloglucan has a branched structure which may contribute to higher release of surface structured water.

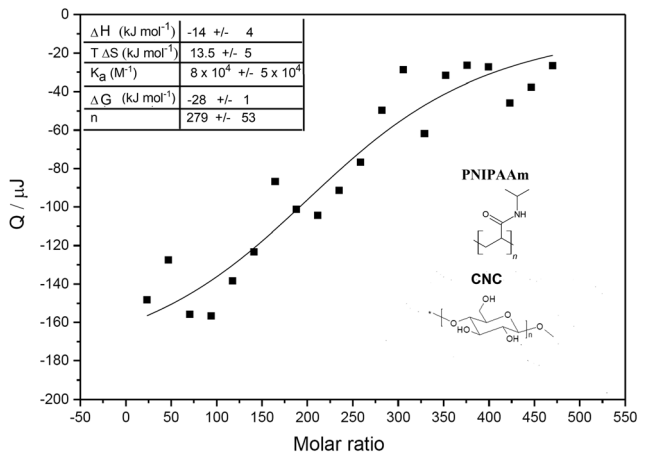

Fig. 2 Isothermal titration calorimetry to study the thermodynamic characteristics of the interaction between CNC and PNIPAAm. Integral plot obtained performing subsequent injections of 10 μL PNIPAAm 3.8 wt% to 0.5 wt% CNC, and fit according to the Levenberg–Marquardt algorithm. Chemical structures of the compounds of interest and values obtained by ITC for the adsorption of PNIPAAm on CNCs.

The value of stoichiometric number n in the titration showed that, on average, 280 PNIPAAm molecules interact with a single CNC rod. The PNIPAAm used has an average molecular weight of 40 kDa, corresponding to 353 repeating units. Considering a surface area per CNC rod to be 3695 nm^2, as previously reported,[26] and the area 0.21 nm^2 for a single anhydroglucose unit, calculated from the crystal structure of cellulose, we calculated 17 600 anhydroglucose units at the surface.[27] As CNCs have 3 H-bond donors for each surface anhydroglucose unit, we can calculate the total number of H-bond donors per rods of 52 786. Taking into account the stoichiometry of the interaction (n = 280) we estimate that each polymer forms up to ≈180 hydrogen bonds with the cellulose surface, involving up to 50% of the repeat units within the PNIPAAm. These calculations support the formation of a strong H-bond network, even if the enthalpy gain associated with a single hydrogen bond is very low (≈0.08 kJ mol^{-1}).[28]

It should be mentioned that the mathematical treatment performed is based on the average stoichiometry of interaction and does not take into account other phenomena that can be associated with irreversible adsorption. We can exclude the formation of covalent linkages, since a chemical equilibrium is a requirement for ITC experiments, but we cannot fully exclude the presence of other possible processes, such as cooperative binding or multilayer formation. The model used to describe ITC data assumes a set of identical binding sites, hence, it did not include these phenomena. It is possible that such secondary processes take place, but that the heat associated is too low to be

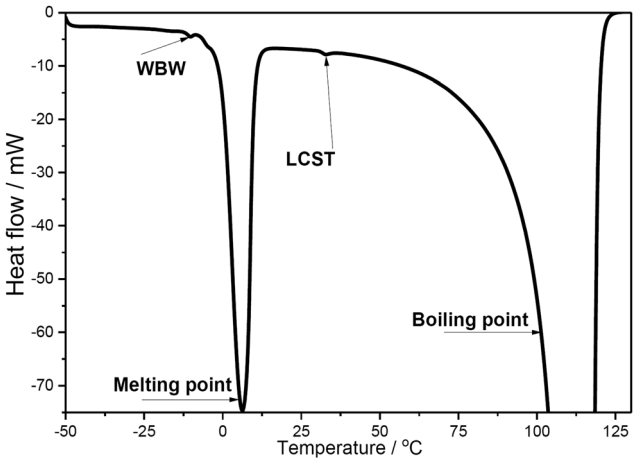

Fig. 3 DSC thermogram of 1 wt% PNIPAAm-3.5 wt% CNC hydrogel.

measurable. In addition, the calculation does not include crosslinking, when a single polymer binds to multiple nanoparticles, which is expected to take place. It should be considered that crosslinking will also occur *via* hydrogen bond formation, so the heat effect will be included in the calorimetric signal. Previous work describing the thermodynamics of ionotropic gelation also included surface interactions and crosslinking as a unique mechanism.[29]

The influence of CNC on the LCST of PNIPAAm in the composite hydrogel was further studied using a DSC that is frequently used to identify various physical properties and thermal transitions of polymeric structures. The results showed that all of the hydrogel samples showed large endothermic reaction at ≈0 °C (melting of the water phase) as well at ≈100 °C (boiling of the water phase), as shown in Fig. 3.

The results showed that the endotherms originating from the water phase, most of the samples contained a small endotherm at 30.5–33.5 °C (see ESI,† Table S-1). This observed temperature region fits nicely with the recorded LCST (lower critical solution temperature) for PNIPAAm (≈32 °C) indicating the temperature where water molecules, hydrogen bonded with the amide groups in PNIPAAm, are released.[30] This conclusion was further supported as the enthalpy of that endotherm increased together with the amount of PNIPAAm. Also, the LCST was not markedly affected by varying the CNC concentration, which can be clearly seen when comparing compositions with highest PNIPAAm concentrations.

In addition, most of the samples also contained minor endotherm at ≈−10 °C which can be linked to the melting of weakly bound water (WBW).[31] The enthalpy values of WBW varied to some extent, especially in compositions with 0.5% CNC (Table S-1, enthalpy values 0–13 J g^{-1}, ESI†). However, any clear correlation with the composition of the studied samples was not observed.

Rheological properties

Fig. 4 illustrates the swelling–deswelling transition of PNIPAAm–CNC hydrogel in various concentrations. The reversibility of the thermal transition was inspected more closely by

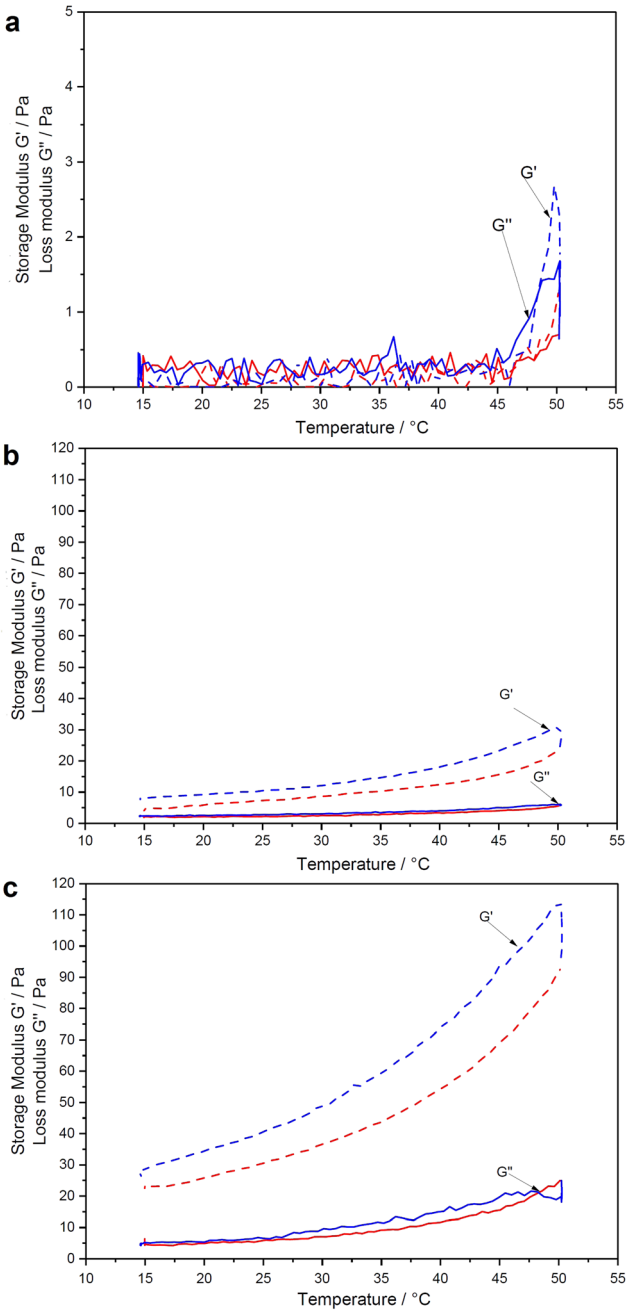

Fig. 4 Rheological analysis of PNIPAAm–CNC hydrogels represented as storage modulus (G') and loss modulus (G'') of hydrogels made within 24 hours from 0.25 wt% PNIPAAm and (a) 0.5 wt%, (b) 3.5 wt%, and (c) 6 wt% CNC. Frequency sweeps were performed at 1% strain and 0.8 rad s^{-1} strain.

imposing heating/cooling cycles from 15 to 50 °C and back to 20 °C, where storage modulus (G') and loss modulus (G'') were measured using fixed frequency and strain values. In all cases a transition from low to higher viscosity was observed as the temperature increased through the transition. According to the cyclic measurements, each material recovered its original G' during cooling, indicating a fully thermoreversible transition. Methylcellulose–CNC hydrogels have shown a similar thermoreversible behavior, but at a broader temperature range from 15

to 70 °C.[18] It is important to note that all rheology data here are affected by the relatively fast temperature ramp (2 K min^{-1}). It causes a lag to the moduli when measured and therefore a sharp transition at the LCST is not observed. However, the stiffening of the gel is evident upon increased temperature.

The noise or outliers were not observed during the rheological analysis, in contrast to the previously reported data for the pure PNIPAAm solutions.[32] Over the entire concentration regime, the temperature-dependence of the linear viscoelastic response can be categorized into three groups; weak softening, strong softening-to-stiffening, and stiffening.[33] These groups correlate to a dramatic non-monotonic evolution of G' trend with heating. Hydrogels containing 0.25 wt% PNIPAAm and 0.5 wt% CNC gave a very weak torque response at the entire temperature range that can be seen in an almost straight trend of a storage modulus (Fig. 4a).

It means that cages used for elastic energy storage appear in small deformations, providing a dominant elastic response. The time of collective relaxation of each cage under small deformation is larger than the experimental time scale, and hence the suspension behaves as a solid ($G' > G''$) on the observational time scales. A slight decrease in the shear moduli can be observed for all hydrogels in the temperature range from 20 to ≈30 °C. A further increase in temperature from 30 to 40 °C leads to non-monotonic trends (softening-to-stiffening) that could be related to heterogeneous clustering of de-swollen polymer chains, which do not form a percolated network.[34] Compared to the pure PNIPAAm that during cooling formed an elongated "bubble" structure due to an even greater lag effect between the temperature ramp and the observed moduli (see ESI,† Fig. S-6), the hydrogels of low PNIPAAm concentration were less stiff and more homogeneous at the maximum onset (Fig. 4a). In a denser network of the pure PNIPAAm solution with many large solid "whity" aggregates which are associated with steric caging and strong physical bonding, longer time is required to obtain steady state.[35,36] The CNCs possibly stabilize the PNIPAAm structure in a hydrogel during heating. Thus, for the biocompatability study, the 0.25 wt% PNIPAAm–3.5 wt% CNC hydrogel was selected due to its intermediate stiffness and ability to be taken with the pipette with the minimal material losses. The cooling leads to the relaxation of the hydrogel network.[37]

Structure-composition dependence of the hydrogel

Unlike SEM, thermoporosimetry enables the detection of the mesoporous (2–50 nm) region in the wet, water-swollen state.[38] Fig. 5 shows the pore size distribution (PSD) of the PNIPAAm–CNC hydrogels as a function of the PNIPAAm or CNC concentrations. A slightly higher moisture content (96.3–96.8%) was observed in hydrogels with 0.25 wt% PNIPAAm compared to other PNIPAAm–CNC hydrogels. However, a nearly constant moisture content (95.7± 0.1%) was determined for 4 wt% PNIPAAm hydrogels when CNC concentrations changed from 0.5 to 6%. Fig. 5a displays bimodal pore size distributions with maxima centred around 3 and 18 nm accounted for 85–90% of total pore volume. This indicates that a large fraction of mesopores of sizes between 1 and

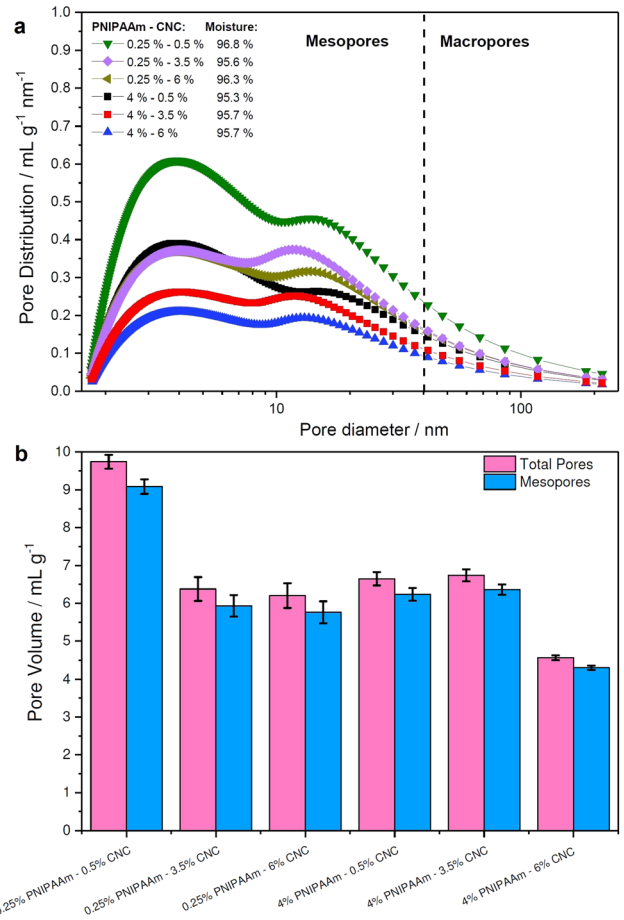

Fig. 5 Quantification of hydrogel porosity. (a) Pore size distribution and (b) pore volume of 0.25 wt% and 4 wt% PNIPAAm-based hydrogels containing 0.5, 3.5, or 6% CNC.

40 nm is located within the hydrogel bridging between larger macropores of size ranging between 40 and 100 nm. Both centred peaks were broad indicating heterogeneity of pore sizes. In summary, the PNIPAAm–CNC hydrogels consist mostly of mesopores with a small fraction of macropores, respectively.

The bimodal design of hydrogel scaffolds was achieved by a strong hydrophilic/hydrophobic contrast between CNCs and PNIPAAm fractions.[39] The cross-linking of CNCs and PNIPAAm leads into a free-standing structure upon osmotic dehydration that leads to enhanced stability and unique mechanical performance, enabling hydrogels with high absorption capacity.[4,40] The limitation of thermoporosimetry is an accurate estimate of only mesopores. Therefore, SEM is often used to characterize the macroporosity of hydrogels.[41]

Fig. 5b illustrates the total pore and mesopores' volumes, where 0.25 wt% PNIPAAm–0.5 wt% CNC hydrogel showed almost twice greater pore volume (10 mL g^{-1}) than 4 wt% PNIPAAm–6 wt% CNC hydrogel (4 mL g^{-1}). Pore volume is smaller in 4 wt% PNIPAAm–6 wt% CNC hydrogel than in other samples. The higher cross-linking density in 4 wt% PNIPAAm–6 wt% CNC hydrogel network decreases the pore volume. The dense cross-linking decreases a distance between

the CNC rods and PNIPAAm which creates an interconnected 3D with pores of a small size. The hydrogels of low concentrations contain a longer distance between PNIPAAm chains and CNCs, and thus, larger pores are expected. The remaining hydrogels showed only slight differences with respect to both total pore and mesopore volume emphasizing the capability of the osmotic dehydration method to allow using both the water interactions and liquid/gas uptakes for forming the molecular assemblies. The low PNIPAAm concentrations allow slower water adsorption but larger penetration *via* capillary forces.[42] With the increasing PNIPAAm concentration, faster water uptake and swelling occur, but the penetration within a hydrogel structure is low. The cryo-TEM analysis shows PNIPAAm–CNC hydrogel that presents a 3D porous structure with sheet-like walls and a relatively smooth surface (see Fig. 6). A highly swollen homogeneous *meso*-porous structure is illustrated revealing a homogeneous distribution of cellular pores over the entire cross-cut hydrogel surface.[43] The interconnected network structure and low viscous structure inside the pores and on the hydrogel surface offer a pathway to use PNIPAAm–CNC hydrogel in biomedical applications. Ideally, hydrogel scaffold used in cell and tissue cultivation should have an interconnected porous structure for cell ingrowth, nutrient transport, waste removal and balanced mechanical strength that mimics the native tissue.[44]

Biocompatibility of hydrogels

While nanocellulose is widely used in biotechnical applications, most of the previous biocompatibility studies were performed using CNF hydrogels.[11] The PNIPAAm–CNC hydrogels were previously tested on injectability and drug-loading capacities, whereas their biocompatibility has not been investigated.[13] To assess the biocompatibility of the hydrogels, fibroblasts were first cultivated in regular cell culture medium on a 96 well plate for 24 h. Isotonic PNIPAAm–CNC hydrogel, CNC dispersion or PNIPAAm solution were applied on top of fibroblasts and 100 μL of medium was applied on top of the hydrogel ((Fig. 7a(2)) schematic). The biocompatibility was studied by cell viability assay, and by assessing the morphology of the cells. The CellTiter-Glo® 3D Cell Viability Assay is based on a luminescence assay. The relative luminescence units (RLU) recorded after two hours for medium control was normalized by setting the luminescence values to 1, and the RLU of all other samples on time points 2 h and 24 h were normalized against the medium control. The mean values of normalized data are shown in Fig. 7b.

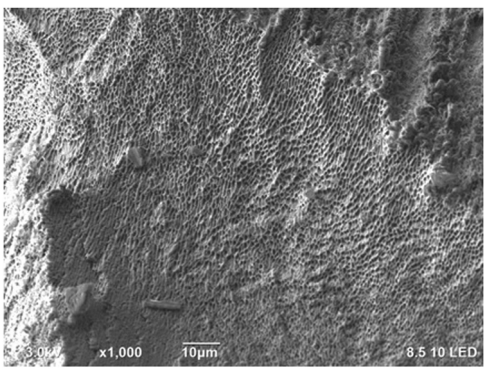

Fig. 6 Cryo TEM analysis of 0.25 wt% PNIPAAm–6 wt% CNC hydrogel.

At time point of two hours, the cell viability was measured to determine the immediate response of cells to these materials. At 2 h, the cell viability was very similar for PNIPAAm–CNC hydrogel (1.0 ± 0.1), PNIPAAm solution (1.1 ± 0.1) and aNFC hydrogel (0.9 ± 0.1) when compared to medium control (1.0 ± 0.0), and statistically significant differences were not observed between them, indicating good biocompatibility of the PNIPAAm–CNC hydrogel. For CNC dispersion (0.5 wt%) instead, the number of cells decreased, being 0.8 ± 0.1 times that of medium control ($p < 0.001$, $n = 9$), which indicates that cells immediately responded to CNC, indicating mild cytotoxicity. Triton X-100 (0.1%) was used as negative control and seemed to kill all cells, as expected, (the number of cells was 0.0 ± 0.0 times that of medium control, $p < 0.001$, $n = 9$). To determine a medium-term exposure to these materials, the cell viability was measured again at 24 h, and medium control sample at 2 h was used as a reference value. Here, slightly larger differences were observed between different samples. For medium control, the number of cells doubled (1.9 ± 0.2) during 22 h culturing whereas for PNIPAAm–CNC hydrogel the number of cells was only 1.6 ± 0.2 times higher as compared to medium control at 2 h. For PNIPAAm solution the number of cells was 2.2 ± 0.3 times higher and for aNFC hydrogel the number of cells was 2.2 ± 0.7 times higher than that of medium control at 2 h.

However, these were not statistically significant differences, indicating similar biocompatibility among these materials. In contrast, for the CNC dispersion, the number of cells at the 24 h time point was only 1.0 ± 0.3 times that of medium control at 2 h ($p < 0.001$, $n = 9$). Therefore, the CNC dispersion seemed to induce a somewhat toxic effect on cells, as ISO 10993-5:2009(E) indicates that a reduction of cell viability by more than 30% is considered a cytotoxic effect.[45] The relative growth of cells, which indicates how different materials influence the proliferation capacity of cells, was determined. The relative growth of cells between 2 and 24 h was analyzed by dividing the RLU measured at 24 h by RLU measured at 2 h. The relative growth at 24 h for medium control was 1.9 ± 0.2, and for PNIPAAm–CNC hydrogel it was lower 1.6 ± 0.1, whereas for CNC dispersion (0.5 wt%) the relative growth was 1.4 ± 0.4. PNIPAAm solution (0.25 wt%) had a relative growth of 2.1 ± 0.2, and for aNFC, relative growth was 2.4 ± 0.9. The differences in relative growth between different samples were not statistically significant due to large variance, but support the idea of good biocompatibility of CNC-PNIPAAm hydrogels.

We also studied how different concentrations of CNC affected the cell viability. By increasing CNC concentration the cell viability slightly decreased when CNC dispersions of 0.5 wt% or 3.5 wt% were compared, as for CNC dispersion (3.5 wt%), the number of cells was 0.6–0.9 times that of CNC dispersion (0.5 wt%), ($n = 3$). Also, PNIPAAm 0.25 wt%–CNC 3.5 wt% hydrogel seemed to induce slightly lower cell viability, being 0.8–0.9 times that of hydrogel containing PNIPAAm 0.25 wt%–CNC 0.5 wt%, ($n = 3$).

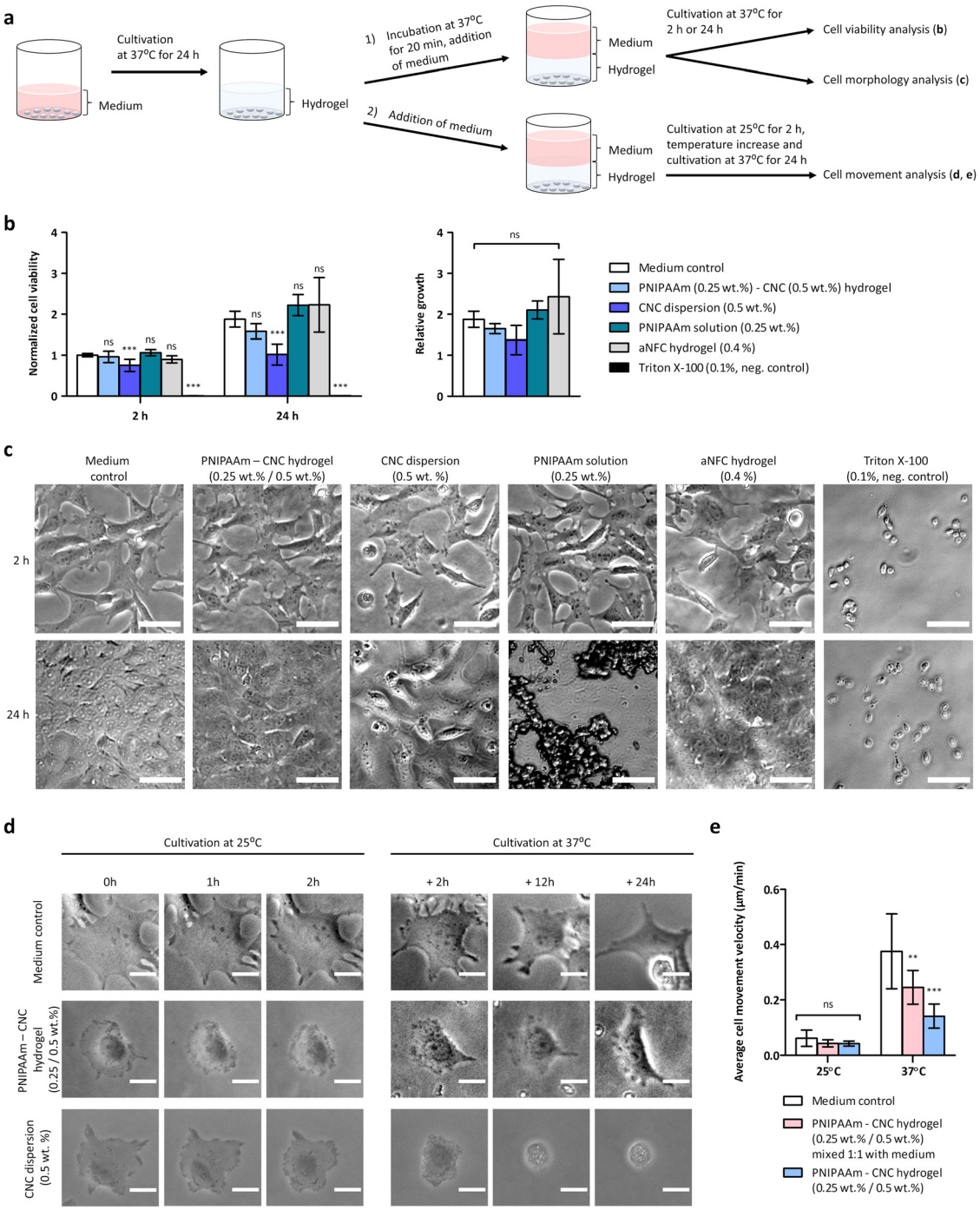

Fig. 7 Biocompatibility of the hydrogel and temperature-mediated actuation of the cells. (a) Schematic of the biocompatibility assay setup. (b) The plate was incubated at 37 °C and the cell viability was determined by CellTiter-Glo 3D cell viability assay after 2 h and 24 h. (c) The morphology of the cells with different materials imaged *via* an optical microscope at different time points, 2 and 24 h. The scale bars are 50 µm. (d) The cell movement was analyzed from time-lapse image series recorded at two different temperatures. The temperature was kept at 25 °C for 2 h and then increased to 37 °C for 24 h. The scale bar is 20 µm. (e) Cell movement velocity was determined at 25 °C and at 37 °C, n = 20 for medium control, n = 10 for PNIPAAm–CNC hydrogel mixed 1 : 1 with medium, and n = 10 for PNIPAAm–CNC hydrogel. Statistical analysis in (b) and (e) was performed by comparing all samples to medium control using one-way ANOVA and Bonferroni's multiple comparison test, * = $p < 0.05$; ** = $p < 0.01$; *** = $p < 0.001$.

The morphology of the cells was assessed by optical microscope. In medium control the cells were nicely spreading after 2 h and after 24 h cells covered the whole surface and formed a confluent layer. After 2 h the spreading of cells seemed very similar for PNIPAAm–CNC hydrogel, aNFC hydrogel and PNIPAAm solutions than in the medium control (Fig. 7c). Similarly, a confluent cell layer was observed after 24 h with PNIPAAm–CNC hydrogel, aNFC hydrogel and PNIPAAm solutions.

Interestingly, when pure PNIPAAm solution was incubated at 37 °C for 24 h, some large aggregates were observed. Physiological salt dispersion induced aggregation of PNIPAAm, and the aggregates in cell culture media may also contain adsorbed serum proteins. However, a confluent cell layer was seen below these aggregates, so the aggregates did not seem to harm cell proliferation (Fig. 7c). The morphology of the cells with CNC dispersion seemed somewhat different than with all other materials, potentially reflecting the cytotoxicity. Already after 2 h, cells cultured in the presence of CNC looked different and, several round cells were observed. Similarly, after 24 h a significant number of round cells were observed although majority of the cells were spreading, and the confluency was about 75%. These results are well in line with the results of the cell viability assay.[46]

Time-lapse imaging was used to study temperature induced changes on hydrogel rheology and consequently on cell behaviour at two different temperatures ((Fig. 7a(2)) schematic). Isotonic PNIPAAm (0.25 wt%)–CNC (0.5 wt%) hydrogel or isotonic CNC (0.5 wt%) dispersion was applied on top of cells and medium was applied as a layer on top of the samples. As a second alternative, isotonic CNC (0.5 wt%) dispersion or PNIPAAm (0.25 wt%)–CNC (0.5 wt%) hydrogel was mixed 1 : 1 with cell culture medium and the mixture was applied on top of cells (see ESI,† Fig. S-2a). At room temperature, both CNC (0.5 wt%) dispersion and PNIPAAm (0.25 wt%)–CNC (0.5 wt%) hydrogel were easily pipettable. The plate was first incubated at 25 °C and 5% CO_2, and time-lapse imaged for 2 h and then the temperature was increased to 37 °C and time-lapse imaging was continued for 24 h. Based on the time-lapse images, it was evident that below CNC dispersion, or CNC dispersion mixed 1 : 1 with medium, the cells were not feeling well, they were not moving much and many cells that were initially spread, started to go round and apoptotic and several cells seemed to die during the experiment (Fig. 7d, see ESI:† Fig. S-2b, Movies S5 and S6). With PNIPAAm (0.25 wt%)–CNC (0.5 wt%) hydrogel cells were moving more, spreading well and communicating with each other (see ESI,† Movie S3). Some salt induced aggregates appeared within the hydrogel, when the temperature was increased to 37 °C. When PNIPAAm (0.25 wt%)–CNC (0.5 wt%) hydrogel was mixed 1 : 1 with medium, the cells were moving and spreading (see ESI,† Fig. S-2b and Movie S4) and in that sense they were looking quite similar than cells in the medium control (Fig. 7d, see ESI,† Movies S1 and S2). However, when hydrogel was mixed 1 : 1 with medium, the opacity increased at 37 °C, which challenged the imaging and decreased the contrast of images. Image series of single cells at different time points below different materials is shown in (Fig. 7d, see ESI:† Fig. S-2b, Movies S1–S6). In PNIPAAm–CNC hydrogels cells were observed to form long-distance mechanical connections, which is an indication of strongly interconnected hydrogel.

At 25 °C the cell movement velocity was 0.06 ± 0.03 μm min^{-1} for medium control ($n = 20$), whereas for both PNIPAAm–CNC hydrogel and PNIPAAm–CNC hydrogel mixed 1 : 1 with medium the cell movement velocity was 0.04 ± 0.01 μm min^{-1} ($n = 10$), and statistically significant differences were not observed. When temperature increased to 37 °C, the cell movement velocity in medium control increased to 0.38 ± 0.14 μm min^{-1} ($n = 20$), but for PNIPAAm–CNC hydrogel the cell movement velocity was significantly lower, 0.14 ± 0.04 μm min^{-1} ($p < 0.001$, $n = 10$), indicating that more viscous hydrogel on top of cells reduced cells ability to move. Cells were also observed to adhere to aggregated particles and move these particles along when cells were moving themselves (see ESI,† Movie S3). When PNIPAAm–CNC hydrogel was mixed 1 : 1 with medium, the cell movement velocity at 37 °C was 0.25 ± 0.06 μm min^{-1} ($p < 0.01$, $n = 10$), which seemed to be well in-between the medium control and PNIPAAm–CNC hydrogel. The movement of individual cells have been tracked to the original live-cell microscopy movies to determine the cell movement velocity (see ESI,† Movies S7–S14). These results suggest that the thermoresponsive nature of the PNIPAAm–CNC hydrogel can be used to control cell movement.

Rationalization of the results

Thermoresponsive PNIPAAm–CNC hydrogels represent an important category of stimuli-responsive materials that rely on changes of LCST to trigger gelation by providing enhanced mechanical properties due to the CNCs integration. The thermo-responsive properties of PNIPAAm can be ascribed to the abrupt transition of molecular chain conformation (linear to coiled) from a hydrophilic to a hydrophobic peripheral structure at the LCST.[47] When the temperature is below the LCST, interactions between PNIPAAm and water are strong, so that hydrogen bonds are formed between the stretched amide groups on the PNIPAAm molecules and the hydroxyl groups on the surface of CNCs. PNIPAAm acted like a binder for CNCs resulting in strong mechanical properties. In this study, the physical interaction between PNIPAAm and CNCs was achieved by entropically driven polymer adsorption of PNIPAAm on CNC surface as well as by hydrogen bonding between the two species. During the osmotic dehydration, the long preparation time could change the hydrogel structure from hydrophilic to hydrophobic as the PNIPAAm–CNC mixture temperature will be higher than the LCST. The negatively charged CNCs can be interspersed between PNIPAAm chains to form a more affluent and stronger pore wall structure and maintain a larger pore size due to the electrostatic repulsion between CNCs leading to a bimodal pore distribution in later measurements. The plenty of hydrophilic hydroxyl and carboxyl groups of CNCs might contribute to improve the water retention of composite PNIPAAm–CNC hydrogel.[48]

CNC hydrogels have been previously shown to be only moderately cytocompatible in several studies.[4,49,50] The literature has reported that a wide range of factors including variation in exposure doses and cellulose source can lead to toxic effects on cells in CNC-based hydrogels.[12] The results of this study showed that CNC dispersion (0.5 wt%) caused some toxic effect on cells. However, when PNIPAAm was mixed with/adsorbed on CNC, the PNIPAAm–CNC hydrogel is biocompatible with cells. The cytotoxicity of CNCs to cells in our study was assigned to the relatively high CNCs concentration (>0.05%) in hydrogels, as discussed previously.[51] However, the mechanical

strength of hydrogels could be ensured only when hydrogels contained CNCs with concentrations >0.5%. Despite the fact that the CNC size can enhance the cytotoxicity of hydrogels to cells, the impact of CNC size was excluded in this study. The CNC used here had smaller length and mean diameter of a cellulose rod (190 ± 50 nm and 7 ± 5 nm) than those in other similar studies.[52] The suitability of PNIPAAm to enhance the biocompatibility of CNC rods of different lengths remains to be studied. Surface charges are important determinants to consider when utilizing CNCs in biocompatibility studies.[53] The CNC-based hydrogels which are fabricated by cation-mediated gelation method have previously shown excellent biocompatibility, in particular when Na^+, Ca^{2+}, Mg^{2+} were selected as gelling cations with the properties to remain stable in an aqueous dispersion for a long time. The low concentrations of gelling cations in CNCs could make hydrogels cytotoxic to cells.

The concentration of CNC played a significant role in the cell biocompatibility – the increase in CNC concentrations from 0.5 wt% or 3.5 wt% decreased the cell viability. The PNIPAAm–CNC hydrogel with 0.5 wt% CNC concentration reached a similar LCST to PNIPAAm.[1] Moreover, the temperature above the LCST led to the well-known morphological transition of PNIPAAm–CNC hydrogel, which induced light scattering and changed the material from transparent to opaque.[54] The temperatures above the LCST in PNIPAAm–CNC hydrogels led to the formation of polymer-rich and polymer-poor micro-phases, forming light-scattering centers.[55] The results of the present study showed that at the temperatures above the LCST the formation of large aggregates representing a PNIPAAm-rich phase did not harm the cell proliferation. The PNIPAAm–CNC hydrogel also contained visible micro-sized fibers representing polymer-poor micro phases, in which cells were still able to make contacts with this network and remained viable. The property of PNIPAAm-based hydrogels turning from transparent to opaque at temperatures above the LCST causes challenges in visualization of the cells below the hydrogel.[56] We believe this could be at least partially solved by using imaging modalities different than visible light and by reducing the length of the light path (for example by using fluorescence imaging from the bottom of the sample).

The knowledge on biocompatibility of hydrogels with relatively "simple" cells such as fibroblasts can be further extended to more complex *in vitro* models, *e.g.*, spheroids, organoids, *etc.* Moreover, additives like nanoparticles and salts, can be blended to the PNIPAAm–CNC hydrogels to provide the required pH, osmolality, and mechanical properties. However, the created biological microenvironment must be assessed according to the requirements of specific cell types. The morphology and size of CNCs are important parameters to consider during the optimization of the PNIPAAm–CNC hydrogel. Despite the fact that in the current study HCl hydrolysis led to defined size distribution of CNCs, the use of other botanical sources for CNCs results in very different mean lengths of CNCs from 50 nm to several microns,[57] have the potential to manufacture cellulose rods of even smaller sizes with narrow shape variance. Thus, the design and architecture of CNCs can be considered as a tunable parameter with respect to mechanical and optical properties leading to improved control over cultured cells or organoids. Overall, the PNIPAAm–CNC showed good biocompatibility and is promising reversibly temperature-modulated hydrogel with chemically defined composition, thus offering potential alternative solution for Matrigel and collagen hydrogels in 3D cell culturing.

Conclusions

Poly(*N*-isopropylacrylamide) (PNIPAAm)–cellulose nanocrystals (CNC) hydrogels were successfully fabricated using osmotic dehydration process. Several hydrogel combinations in various concentrations were further benchmarked to be used as a hydrogel substrate for 3D cell culture. A combination of PNIPAAm–CNC in the concentration of 0.25 wt% and 0.5 wt% enabled excellent mechanical properties due to their thermoresponsive functionality and the small size of CNCs. The hydrogels were synthesized using the osmotic dehydration method without additives. The cross-linked structure of PNIPAAm–CNC hydrogel was confirmed by the formation of an endothermic region, which was hypothetically ascribed to a specific hydrogen bonding between the hydroxyl and carboxylic groups of CNCs and the carbonyl oxygen or the amide group of PNIPAAm. We observed improved biocompatibility of the PNIPAAm–CNC hydrogel over CNC alone. Furthermore, the thermoresponsive material enabled influencing cell behavior, namely cell movement, with temperature changes, but the simultaneous changes in the optical properties of the hydrogel caused technical difficulties in imaging. Controlling the mechanical properties of the hydrogel by temperature may enable applications such as enhanced 3D printing. Therefore, more work is needed to improve the optical properties of hydrogels at temperatures above LCST while maintaining the mechanical stability and biocompatibility. This could be achieved by engineering CNCs of smaller size or with different shape using other hydrolysis treatment. The suitability of these hydrogels as microenvironments for the culturing of more complicated tissue models such as organoids or tumor spheroids remains to be individually assessed in future studies.

Conflicts of interest

There are no conflicts to declare.

Acknowledgements

The authors would like to acknowledge the Academy of Finland for the financial support by project NanOrganoid (project 337580). Prof. Hytönen and Dr Leppiniemi acknowledge the Biocenter Finland and Tampere Imaging Facility for the service, and thank Niklas Kähkönen and Janne Kärnä (Tampere University) for excellent technical support. Prof. Thielemans and Dr Lombardo thank KU Leuven for funding through SL's PostDoctoral Mandate (grant PDMT 1/21/017) and project C14/18/061. Dr Trubetskaya acknowledges Nansenfondet Oslo Norway for the financial support (project 1051).

References

1 X. Sun, P. Tyagi, S. Agate, L. Lucia, M. McCord and L. Pal, Unique thermo-responsivity and tunable optical performance of poly(*N*-isopropylacrylamide)–cellulose nanocrystal hydrogel films, *Carbohydr. Polym.*, 2019, **208**, 495–503, DOI: 10.1016/j.carbpol.2018.12.067.

2 J. Wang, Q. Cheng, S. Feng, L. Zhang and C. Chang, Shear-aligned tunicate-cellulose-nanocrystal-reinforced hydrogels with mechano-thermo-chromic properties, *J. Mater. Chem. C*, 2021, **9**, 6344–6350, DOI: 10.1039/d1tc00911g.

3 E. Gicquel, C. Martin, L. Heux, B. Jean and J. Bras, Adsorption versus grafting of poly(*N*-Isopropylacrylamide) in aqueous conditions on the durface of cellulose nanocrystals, *Carbohydr. Polym.*, 2019, **210**, 100–109, DOI: 10.1016/j.carbpol.2019.01.022.

4 K. J. De France, T. Hoare and E. D. Cranston, Review of Hydrogels and Aerogels Containing Nanocellulose, *Chem. Mater.*, 2017, **29**, 4609–4631, DOI: 10.1021/acs.chemmater.7b00531.

5 K. Nagase, Thermoresponsive interfaces obtained using poly(*N*-isopropylacrylamide)-based copolymer for bioseparation and tissue engineering applications, *Adv. Colloid Interface Sci.*, 2021, **295**, 102487, DOI: 10.1016/j.cis.2021.102487.

6 J. O. Zoppe, Y. Habibi, O. J. Rojas, R. A. Venditti, L. S. Johansson and K. Efremenko, *et al.*, Poly(*N*-isopropylacrylamide) brushes grafted from cellulose nanocrystals vis surface-initiated single-electron transfer living radical polymerization, *Biomacromol.*, 2010, **11**(10), 2683–2691, DOI: 10.1021/bm100719d.

7 J. A. Kelly, A. M. Shukaliak, C. C. Y. Cheung, K. E. Shopsowitz, W. Y. Hamad and M. J. MacLachlan, Responsive photonic hydrogels based on nanocrystalline cellulose, *Angew. Chem., Int. Ed.*, 2013, **52**(34), 8912–8916, DOI: 10.1002/anie.201302687.

8 J. Tang, R. M. Berry and K. C. Tam, Stimuli-Responsive Cellulose Nanocrystals for Surfactant-Free Oil Harvesting, *Biomacromolecules*, 2016, **17**(5), 1748–1756, DOI: 10.1021/acs.biomac.6b00144.

9 A. Hebeish, S. Farag and T. I. Shaheen, Thermal responsive hydrogels based on semi interpenetrating network of poly(NIPAm) and cellulose nanowhiskers, *Carbohydr. Polym.*, 2014, **102**, 159–166, DOI: 10.1016/j.carbpol.2013.10.054.

10 M. Tagliazucchi, O. Azzaroni and I. Szleifer, Responsive Polymers End-Tethered in Solid-State Nanochannels: When Nanoconfinement Really Matters, *J. Am. Chem. Soc.*, 2010, **132**(35), 12404–12411, DOI: 10.1021/ja104152g.

11 K. Heise, E. Kontturi, O. Ikkala, Nonappa, Y. Allahverdiyeva, T. Tammelin and M. B. Lindner, Nanocellulose: Recent fundamental advances and emerging biological and biomimicking applications, *Development*, 2020, **33**(3), 2004349, DOI: 10.1002/adma.202004349.

12 N. Stoudmann, M. Schmutz, C. Hirsch, B. Nowack and C. Som, Human hazard potential of nanocellulose: quantitative insights from the literature, *Nanotox.*, 2020, **14**(9), 1241–1257, DOI: 10.1080/17435390.2020.1814440.

13 K. Zubik, P. Singhsa, Y. Wang, H. Manuspiya and R. Narain, Thermo-Responsive Poly(*N*-Isopropylacrylamide) Cellulose Nanocrystals Hybrid Hydrogels for Wound Dressing, *Polymers*, 2017, **9**(19), 1–17, DOI: 10.3390/polym9040119.

14 R. Curvello, V. S. Raghuwanshi and G. Ganier, Engineering nanocellulose hydrogels for biomedical applications, *Adv. Colloid Interface Sci.*, 2019, **267**, 47–61, DOI: 10.1016/j.cis.2019.03.002.

15 T. Pääkkönen, P. Spiliopoulos, A. Knuts, K. Nieminen, L. S. Johansson and E. Kontturi, *et al.*, From vapour to gas: optimising cellulose degradation with gaseous HCl, *React. Chem. Eng.*, 2018, **3**, 312–318, DOI: 10.1039/C7RE00215G.

16 V. Guccini, J. Phiri, J. Trifol, V. Rissanen, T. Tammelin and E. Kontturi, *et al.*, Tuning the Porosity, Water Interaction, and Redispersion of Nanocellulose Hydrogels by Osmotic Dehydration, *ACS Appl. Polym. Mater.*, 2022, **4**, 24–28, DOI: 10.1021/acsapm.1c01430.

17 Z. Liu, H. Choi, P. Gatenholm and A. R. Esker, Quartz Crystal Microbalance with Dissipation Monitoring and Surface Plasmon Resonance Studies of Carboxymethyl Cellulose Adsorption onto Regenerated Cellulose Surfaces, *Langmuir*, 2011, **27**, 8718–8728, DOI: 10.1021/la200628a.

18 J. R. McKee, S. Hietala, J. Seitsonen, J. Laine, E. Kontturi and O. Ikkala, Thermoresponsive Nanocellulose Hydrogels with Tunable Mechanical Properties, *ACS Macro Lett.*, 2014, **161**, 266–270, DOI: 10.1021/mz400596g.

19 S. Lombardo and W. Thielemans, Thermodynamics of the interactions of positively charged cellulose nanocrystals with molecules bearing different amounts of carboxylate anions, *Phys. Chem. Chem. Phys.*, 2018, **26**, 17637–17647, DOI: 10.1039/C8CP01532E.

20 W. Xu, H. Baribault and E. D. Adamson, Vinculin knockout results in heart and brain defects during embryonic development, *Development*, 1998, **125**(2), 327–337, DOI: 10.1242/dev.125.2.327.

21 K. S. Kontturi, E. Kontturi, T. Tammelin, P. Stenius and L. S. Johansson, Adsorption of Cationic Starch on Cellulose Studied by QCM-D, *Langmuir*, 2008, **24**, 4743–4749, DOI: 10.1021/la703604j.

22 E. Kontturi, T. Tammelin and M. Österberg, Cellulose – model films and the fundamental approach, *Chem. Soc. Rev.*, 2006, **35**, 1287–1304, DOI: 10.1007/978-3-319-76573-0-6-1.

23 G. Gicquel, *PhD development of stimuli-responsive cellulose nanocrystals hydrogels for smart applications*, 2017.

24 S. Lombardo and W. Thielemans, Thermodynamics of adsorption on nanocellulose surfaces, *Cellulose*, 2019, **26**, 249–279, DOI: 10.1007/s10570-018-02239-2.

25 S. Kishani, T. Benselfelt, L. WÅgberg and J. Wohlert, Entropy drives the adsorption of xyloglucan to cellulose surfaces – a molecular dynamics study, *J. Colloid Interface Sci.*, 2021, **588**, 485–493, DOI: 10.1016/j.jcis.2020.12.113.

26 S. Lombardo, W. Thielemans, S. Eyley, C. Schütz, H. van Gorp and S. Rosenfeldt, *et al.*, Thermodynamic Study of the Interaction of Bovine Serum Albumin and Amino Acids with Cellulose Nanocrystals, *Langmuir*, 2017, **33**(22), 5473–5481, DOI: 10.1021/acs.langmuir.7b00710.

27 Y. Nishiyama, J. Sugiyama, H. Chanzy, C. Schütz, H. van Gorp and P. Langan, Crystal Structure and Hydrogen Bonding System in Cellulose Iα from Synchrotron X-Ray and

Neutron Fiber Diffraction, *J. Am. Chem. Soc.*, 2003, **125**(47), 14300–14306, DOI: 10.1021/ja0257319.

28 E. Freira, Do enthalpy and entropy distinguish first in class from best in class?, *Drug Discovery Today*, 2008, **13**(19–20), 869–874, DOI: 10.1016/j.drudis2008.07.005.

29 S. Lombardo, A. Gencer, C. Schütz, J. Van Rie, S. Eyley and W. Thielemans, Thermodynamic study of ion-driven aggregation of cellulose nanocrystals, *Biomacromolecules*, 2019, **20**(8), 3181–3190, DOI: 10.1021/acs.biomac.9b00755.

30 E. R. Gariepy and J. C. Leroux, In situ-forming hydrogels – review of temperature – sensitive systems, *Eur. J. Pharm. Biopharm.*, 2004, **58**(2), 409–426, DOI: 10.1016/j.ejpb.2004.03.019.

31 V. M. Gunko, I. N. Savina and S. V. Mikhalovsky, Properties of Water Bound in Hydrogels, *Gels*, 2017, **3**(4), 1–30, DOI: 10.3390/gels3040037.

32 G. Chaudhary, A. Ghosh, J. G. Kang, P. V. Braun, R. H. Ewolt and K. Schweizer, Linear and nonlinear viscoelasticity of concentrated thermoresponsive microgel suspensions, *J. Colloid Interface Sci.*, 2021, **601**, 886–898, DOI: 10.1016/j.jcis.2021.05.111.

33 A. Ghosh, G. Chaudhary, J. G. Kang, P. V. Braun, R. H. Ewolt and K. Schweizer, Linear and nonlinear rheology and structural relaxation in dense glassy and jammed soft repulsive pNIPAM microgel suspensions, *Soft Matter*, 2019, **15**, 1038–1052, DOI: 10.1039/C8SM02014K.

34 A. Town, E. Niezabitowska, J. Kavanagh, M. Barrow, V. R. Kearns and T. O. McDonald, Understanding the Phase and Morphological Behavior of Dispersions of Synergistic Dual-Stimuli-Responsive Poly(*N*-isoropylacrylamide) Nanogels, *J. Phys. Chem. B*, 2019, **123**, 6303–6313, DOI: 10.1021/acs.jpcb.9b04051.

35 M. Jaspers, M. Dennison, M. F. J. Mabesoone, F. C. MacKintosh, A. E. Rowan and P. H. J. Kouwer, Ultra-responsive soft matter from strain-stiffening hydrogels, *Nat. Commun.*, 2014, **5**(5808), 1–8, DOI: 10.1038/ncomms6808.

36 G. M. Conley, P. Aebischer, S. Nöjd, P. Schurtenberger and F. Scheffold, Jamming and overpacking fuzzy microgels: Deformation, interpenetration, and compression, *Sci. Adv.*, 2017, **3**, 1–8, DOI: 10.1126/sciadv.17009.

37 P. de Almeida, *PhD Biomimetic Hydrogels under Stress*, 2020.

38 I. S. Raja and N. N. Fathima, Porosity and dielectric properties as tools to predict drug release trends from hydrogels, *SpringerPlus*, 2014, **393**, 1–10, DOI: 10.1186/2193-1801-3-393.

39 X. Y. Yang, Y. Li, X. Liu, A. Lemaire, J. G. Yu and B. L. Su, Hierarchically structured functional materials: synthesis strategies for multimodal porous networks, *Pure Appl. Chem.*, 2009, **81**(12), 2265–2307, DOI: 10.1351/PAC-CON-09-05-06.

40 J. Ju, Z. Gu, X. Liu, S. Zhang, X. Peng and T. Kuang, Fabrication of bimodal open-porous poly(butylene succinate)/cellulose nanocrystals composite scaffolds for tissue engineering application, *Int. J. Biol. Macromol.*, 2020, **147**, 1164–1173, DOI: 10.1016/j.ijbiomac.2019.10.085.

41 P. Orsolini, B. Michen, A. Huch, P. Tingaut, W. R. Caseri and T. Zimmermann, Characterization of Pores in Dense Nanopapers and Nanofibrillated Cellulose Membranes: A Critical Assessment of Established Methods, *ACS Appl. Mater. Interfaces*, 2015, **7**, 25884–25897, DOI: 10.1021/acsami.5b08308.

42 R. Ajdary, B. L. Tardy, B. D. Mattos, L. Bai and O. J. Rojas, Plant Nanomaterials and Inspiration from Nature: Water Interactions and Hierarchically Structured Hydrogels, *Adv. Mater.*, 2020, **33**(28), 2001085, DOI: 10.1002/adma.202001085.

43 Z. Kaberova, E. Karpushkin, M. Nevoralova, M. Vetrik, M. Slouf and M. Duskova-Smrskova, Microscopic Structure of Swollen Hydrogels by Scanning Electron and Light Microscopies: Artifacts and Reactivity, *Polymers*, 2020, **12**(578), 1–18, DOI: 10.3390/polym12030578.

44 S. H. Aswathy, U. Narendrakumar and I. Manjubala, Commercial hydrogels for biomedical applications, *Heliyon*, 2020, **6**(4), e03719, DOI: 10.1016/j.heliyon.2020.e03719.

45 ISO 10993-5:2009, Biological evaluation of medical devices – part 5: Tests for in vitro cytotoxicity (2009), DOI: 10.1242/dev.125.2.327.

46 L. A. Gurski, A. K. Jha, C. Zhang, X. Jia and M. C. Farach-Carson, Hyaluronic Acid-Based Hydrogels as 3D Matrices for in Vitro Evaluation of Chemotherapeutic Drugs Using Poorly Adherent Prostate Cancer Cells, *Biomaterials*, 2009, **30**(30), 6076–6085, DOI: 10.1016/biomaterials.2009.07.054.

47 X. Zhang, Y. Wang, J. Zhao, M. Xiao, W. Zhang and C. Lu, Mechanically Strong and Thermally Responsive Cellulose Nanofibers Poly(*N*-isopropylacrylamide) Composite Aerogels, *ACS Sustainable Chem. Eng.*, 2016, **4**, 4321–4327, DOI: 10.1021/acssuschemeng.6b00814.

48 H. Ma, Y. Zou, S. Zhang, L. Liu, J. Yu and Y. Fan, Nanochitin and poly(*N*-isopropylacrylamide) interpenetrating network hydrogels for temperature sensor applications, *Carbohydr. Polym.*, 2022, **291**, 119544, DOI: 10.1016/j.carbpol.2022.119544.

49 J. Catalan, E. Rydman, K. Aimonen, K. S. Hannukainen, S. Suhonen and E. Vanhala, *et al.*, Genotoxic and inflammatory effects of nanofibrillated cellulose in murine lungs, *Mutagenesis*, 2017, **32**, 23–31, DOI: 10.1093/mutage/gew035.

50 G. K. Tummala, V. R. Lopes, N. Ferraz and A. Mihranyan, Biocompatibility of Nanocellulose-Reinforced PVA Hydrogel with Human Corneal Epithelial Cells for Ophthalmic Applications, *J. Funct. Biomater.*, 2019, **10**(3), 1–10, DOI: 10.3390/jfb10030035.

51 S. Dong, A. A. Hirani, K. R. Colacino, Y. W. Lee and M. Roman, Cytotoxicity and cellular update of cellulose nanocrystals, *Nano LIFE*, 2012, **2**, 1241006, DOI: 10.1142/S1793984412410061.

52 Z. Hanif, F. R. Ahmed, S. W. Shin, Y. K. Kim and S. H. Um, Size and dose-dependent toxicity of cellulose nanocrystals (cnc) on human fibroblasts and colon adenocarcinoma, *Colloids Surf., B*, 2014, **119**, 162–165, DOI: 10.1016/j.colsurfb.2014.04.018.

53 S. Meschini, E. Pellegrini, C. A. Maestri, M. Condello, P. Bettotti, G. Condello and M. Scarpa, In vitro toxicity assessment of hydrogel patches obtained bycation-induced cross-linking of rod-like cellulose nanocrystals, *Biomed. Mater. Res.*, 2020, **108B**, 687–697, DOI: 10.1002/jbm.b.34423J.

54 Y. Cao, L. Lewis, W. Y. Hamad and M. J. MacLachlan, Pressure-responsive hierarchical chiral photonic aerogels, *Adv. Mater.*, 2019, **31**(21), 1808186, DOI: **10.1002/adma.201808186**.
55 A. Eklund, H. Zhang, H. Zeng, A. Priimagi and O. Ikkala, Fast Switching of Bright Whiteness in Channeled Hydrogel Networks, *Adv. Funct. Mater.*, 2020, **30**, 2000754, DOI: **10.1002/adfm.202000754**.
56 M. Zhuang, T. Liu, K. Song, D. Ge and X. Li, Thermo-responsive poly(*N*-isopropylacrylamide)-grafted hollow fiber membranes for osteoblasts culture and non-invasive harvest, *Mater. Sci. Eng., C*, 2015, **55**, 410–419, DOI: **10.1016/j.msec.2015.05.040**.
57 Y. Tang, H. Yang and S. Vignolini, Recent Progress in Production Methods for Cellulose Nanocrystals: Leading to More Sustainable Processes, *Adv. Sust Systems*, 2022, **6**(3), 1–16, DOI: **10.1002/adsu.202100100**.